frontiers in Electronics

ORIGINAL RESEARCH
published: 22 March 2022
doi: 10.3389/felec.2022.813535

# Solution-Processed Titanium Dioxide Ion-Gated Transistors and Their Application for pH Sensing

*Arunprabaharan Subramanian[1], Mona Azimi[1], Cheng Yee Leong[2], Siew Ling Lee[2], Clara Santato[3] and Fabio Cicoira[1]**

[1]Department of Chemical Engineering, Polytechnique Montréal, Montreal, QC, Canada, [2]Department of Chemistry, University of Technology Malaysia, Johor Bahru, Malaysia, [3]Department of Engineering Physics, Polytechnique Montréal, Montreal, QC, Canada

Titanium dioxide ($TiO_2$) is an abundant metal oxide, widely used in food industry, cosmetics, medicine, water treatment and electronic devices. $TiO_2$ is of interest for next-generation indium-free thin-film transistors and ion-gated transistors due to its tunable optoelectronic properties, ambient stability, and solution processability. In this work, we fabricated $TiO_2$ films using a wet chemical approach and demonstrated their transistor behavior with room temperature ionic liquids and aqueous electrolytes. In addition, we demonstrated the pH sensing behavior of the $TiO_2$ IGTs with a sensitivity of ~48 mV/pH. Furthermore, we demonstrated a low temperature (120°C), solution processed $TiO_2$-based IGTs on flexible polyethylene terephthalate (PET) substrates, which were stable under moderate tensile bending.

**Keywords: titanium dioxide, ion-gating, transistors, pH sensors, thin films**

OPEN ACCESS

***Edited by:***
*Luisa Petti,*
*Free University of Bozen-Bolzano, Italy*

***Reviewed by:***
*Mattia Petrelli,*
*Free University of Bozen-Bolzano, Italy*
*Giulia Casula,*
*University of Cagliari, Italy*

****Correspondence:***
*Fabio Cicoira*
*fabio.cicoira@polymtl.ca*

***Specialty section:***
*This article was submitted to Flexible Electronics, a section of the journal Frontiers in Electronics*

***Received:*** *11 November 2021*
***Accepted:*** *02 March 2022*
***Published:*** *22 March 2022*

***Citation:***
*Subramanian A, Azimi M, Leong CY, Lee SL, Santato C and Cicoira F (2022) Solution-Processed Titanium Dioxide Ion-Gated Transistors and Their Application for pH Sensing. Front. Electron. 3:813535. doi: 10.3389/felec.2022.813535*

## INTRODUCTION

Oxide semiconductors are commonly used in display technologies, energy conversion as well as chemo- and bio-sensing, due to their remarkable physicochemical properties, tunable optoelectronic behavior and mixed ionic-electronic conductivities (Manjakkal et al., 2020; Rim, 2020; Wager, 2020; Papac et al., 2021; Shi et al., 2021; Yoo et al., 2021). They are cost-effective, transparent to visible light, stable in ambient conditions and solution-processable at low temperatures in ambient air (Park et al., 2020; Tiwari et al., 2020). Oxide semiconductors are extensively studied as active channel materials for field-effect transistors (FETs) and ion-gated transistors (IGTs) (Wager, 2016; Cadilha Marques et al., 2019; Leighton, 2019), where charge carrier mobility, ON/OFF current ratio, operating voltage and switching speed are key parameters for determining device performance. Amorphous indium gallium zinc oxide (IGZO), showing a mobility above 10 $cm^2$/Vs, is already used in organic light emitting diode (OLED) display backplanes (Nomura et al., 2004; Wager, 2016; Ji et al., 2021; Song et al., 2021). However, due to the scarcity of indium in the earth's crust, several alternative oxide semiconductors are being explored (Ramarajan et al., 2020). For instance, in addition to display technologies, the earth-abundant materials ZnO, $SnO_2$ and $TiO_2$ are investigated for sensor applications (Nunes et al., 2019; Manjakkal et al., 2020; Şerban and Enesca, 2020; Sedki et al., 2021). To develop sensors for physiological (e.g., point-of-care testing) and environmental monitoring (e.g., water quality monitoring), the semiconductors need to be stable in ambient conditions (Rim, 2020). $TiO_2$ is known for its abundancy, non-toxicity, tunable optoelectronic properties, high stability under ambient conditions and biocompatibility (Chen and Selloni, 2014). Depending on the type of synthesis, thermal treatment temperature, and type of gating media, FETs

and IGTs based on $TiO_2$ channels exhibit charge carrier mobility ranging from 0.05 to 10 $cm^2$/Vs (Zhong et al., 2012; Chong and Kim, 2013; Horita et al., 2013; Valitova et al., 2016; Yajima et al., 2016; Tiwale et al., 2020; Zhang et al., 2021).

Various film processing routes lead to different morphologies, crystal structures and chemical compositions of $TiO_2$, resulting in different electrical properties (Anitha et al., 2015). $TiO_2$ can be processed *via* a variety of sustainable wet chemical approaches, such as spin-coating, dip-coating, spray-coating and printing (Thomas et al., 2013). However, the high processing temperature (>250°C) and brittle nature of metal oxide films limit their applicability in flexible and stretchable electronics (De A. Freire et al., 1999; Zardetto et al., 2011; Moonen et al., 2012; Wang et al., 2019; Asare et al., 2020; Baeg and Lee, 2020; Park et al., 2020).

Metal oxide-based IGTs employ semiconducting metal oxides as active channel materials and ionic liquids, ion-gels or aqueous saline solutions as the ion-gating media (Kim et al., 2013; Bisri et al., 2017; Cadilha Marques et al., 2019; Huang et al., 2021; Subramanian et al., 2021). Due to its autoionization, deionized (DI) water can also be used as gating medium (Singh et al., 2016). IGTs operate at low voltages, due to the formation of an electrical double layer at the oxide semiconductor/ion-gating medium interface (Bisri et al., 2017; Griffin, 2020). Current modulation in IGTs can be explained by electrostatic (surface) and electrochemical (volumetric) doping. Surface doping is achieved by the migration of ions from the gating medium towards the surface of the semiconductor and subsequent formation of a high-capacitance electrical double layer, whereas volumetric doping is achieved when ions from the gating medium pass through the permeable surface into the bulk of the semiconductor (Laiho et al., 2011; Kim et al., 2013; Bisri et al., 2017; Sood et al., 2021; Torricelli et al., 2021). Horita et al. (2013) fabricated anatase $TiO_2$-based IGTs using ionic liquids, ion-gels and polyvinyl alcohol and investigated the transistor performance with different mobile ions in the ion-gating media. We recently demonstrated that the characteristics of IGTs based on porous and compact $TiO_2$ films gated by pure 1-ethyl-3-methylimidazolium bis(trifluoromethylsulfonyl)imide ([EMIM][TFSI]), and $Li^+$ ions in [EMIM] [TFSI] were significantly affected by the film morphology and the gating medium (Subramanian et al., 2020).

IGTs can be used as chemical sensors and biosensors due to their ability to function as ion/electron converters (Bu et al., 2020; Torricelli et al., 2021). In IGT sensors, the analyte, i.e., substance to be detected, can be included in the gating medium, leading to a change of the electronic signal (Bu et al., 2020; Cea et al., 2020; Rim, 2020). In IGTs, the analyte is in direct contact with semiconductor, while in the case of ion-sensitive field-effect transistor (ISFETs), it is in direct contact with the gate dielectric. The low operating voltage of oxide-based IGTs makes possible the detection of biomolecules that feature undesired redox reactions at high voltages. In addition, surface functionalization of the oxide semiconductor permits functionalization with specific chemical/biological species. As an example, the surface functionalization of ZnO with the glucose oxidase enzyme enabled the specific quantitative detection of D-glucose in IGT configuration (Bandiello et al., 2014). The detection of coronavirus and cancer biomarkers were recently reported using oxide IGTs (Ishikawa et al., 2009; Chang et al., 2011; AlQahtani et al., 2021).

Oxide-based IGTs can be used as pH sensors, exploiting the threshold voltage shift induced by changes in the pH of the gating medium (Kergoat et al., 2010; Bhatt et al., 2020; Lee et al., 2020). Previous reports based on $TiO_2$ extended-gate ISFETs showed a maximum pH sensitivity of 60 mV/pH (Li et al., 2014; Yao et al., 2014; Yusof et al., 2016; Zulkefle et al., 2016). These devices are composed of a FET (transducing unit), a sensing unit and control gate electrode. The sensing unit and the control gate are placed in the environment containing the analyte solution and the sensing unit is remotely connected to the gate terminal of the FET which is placed outside the analyte. (Li et al., 2014).

In this work, we synthesized $TiO_2$ films using a sustainable wet chemical method employing green alcohol solvents (isopropanol and ethanol). We demonstrated the successful operation of $TiO_2$ IGTs at low voltages in an ionic liquid and an aqueous saline solution. $TiO_2$ IGTs were also used as pH sensors with a pH sensitivity of ~48 mV/pH. Due to the *n*-type nature of the $TiO_2$ film, the increase of $[H]^+$ (decrease of pH) makes the IGTs turn on at lower voltages. Conversely, the IGTs turn on at higher voltages at higher pH. In addition, we fabricated $TiO_2$ films on flexible PET substrates at the maximum processing temperature of 120°C and showed that their performance was not severely affected under tensile bending state.

# EXPERIMENTAL

## Film Deposition

The solution for $TiO_2$ sol-gel synthesis on rigid substrates (route I) was prepared by mixing 1.7 ml of titanium butoxide (Alfa Aesar, 99%), 65 µL of concentrated $HNO_3$ (Thermo Fisher Scientific, 70%), 90 µL of deionized water (Milli-Q water purification system, resistivity of 18.2 MΩ cm) and 19.1 ml of isopropyl alcohol (HoneyWell, 99.9%) for 6 h at room temperature (Kajitvichyanukul et al., 2005; Parthiban et al., 2015). This solution was spin-coated on Au/Ti (40 nm/5 nm) pre-patterned $SiO_2$/*p*-Si (200 nm/500 µm) substrates (Wafer Pro, Santa Clara, CA, United States) at 2,000 rpm for 40 s. The films were heated initially at 100°C for 15 min to evaporate the solvents and subsequently in a tubular furnace in ambient air (Thermolyne 21100) at 450 ± 10°C for 1 h (Parthiban et al., 2015).

$TiO_2$ films on flexible PET substrates were obtained with a different method (route II), which only required a thermal treatment at 120°C. A $TiO_2$ suspension was prepared by mixing 10 g of Aeroxide $TiO_2$ P25 nanoparticles (Photocatalytic standard, particle size ~21 nm, Millipore Sigma), 107 ml of ethanol (Commercial Alcohols Inc., Canada), 1.4 ml of deionized water and 3.7 ml of titanium tetraisopropoxide (Millipore Sigma) overnight at room temperature. This suspension was spin-coated on Au/Ti (40 nm/5 nm) pre-patterned polyethylene terephthalate (PET) substrates (175 µm thick, antistatic coating on both sides, purchased from Policrom Inc., Bensalem, PA, United States)

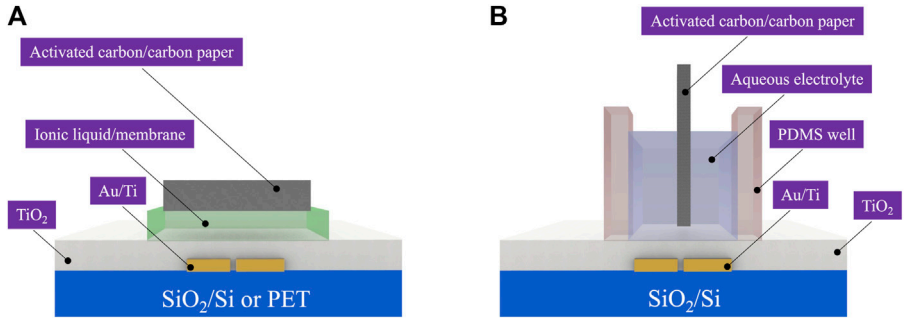


**SCHEME 1 |** Device schemes of **(A)** ionic liquid and **(B)** aqueous electrolyte gated $TiO_2$ transistors.

at 4,000 rpm for 40 s. The films were heated at 120°C for 90 min in ambient air (Kim and Hwang, 2014).

## Film Characterization

The topographical characteristics of the $TiO_2$ films were analyzed using tapping-mode atomic force microscopy (AFM) performed with a Digital Instruments Dimension 3100 and JPK NanoWizard 3 equipped with a silicon cantilever (Spring constant: 40 N/m, tip radius: <10 μm and resonance frequency: 300 kHz). The thicknesses of the $TiO_2$ films (~55 nm for route I films and ~1.1 μm for route II films) were measured using a profilometer (Dektak 150, Veeco, Plainview, NY, United States). The morphological characteristics of the $TiO_2$ films were analyzed using JEOL JSM-7600F and Hitachi SU8020 field emission scanning electron microscopes (FESEM). The crystal structures of the $TiO_2$ films were analyzed using X-ray diffraction (XRD) performed with Bruker D8 and Rigaku SmartLab diffractometers using CuKα source. The x-rays were scanned (1°/minute) from $2\theta = 10^{\circ}$ to $2\theta = 60^{\circ}$.

## Device Fabrication

Photolithographically patterned Au/Ti (40 nm/5 nm) source and drain electrodes (width/length = 4,000 μm/10 μm) on $SiO_2$/p-Si and PET substrates were prepared according to a procedure described previously (Valitova et al., 2016; De Oliveira Silva et al., 2019; Subramanian et al., 2021). The patterned substrates were ultrasonically cleaned using sequential baths of isopropyl alcohol, acetone and isopropyl alcohol and exposure to UV-ozone for 15 min, prior to the deposition of the $TiO_2$ films (Subramanian et al., 2020).

For ionic liquid gating, a PVDF (polyvinylidene fluoride, 220 nm pore size, Millipore Sigma) membrane (9 × 4 mm) soaked with [EMIM] [TFSI] (IoLiTec Ionic Liquids Technologies GmbH, Germany) was placed on the top of the $TiO_2$ layer and served as the ion-gating media. Activated carbon on carbon paper (6 × 3 mm) was used as the gate electrode and manually placed on top of the ion-gating medium to complete the fabrication of the ionic liquid-gated transistor (Subramanian et al., 2020; Azimi et al., 2021; Subramanian et al., 2021).

For aqueous electrolyte gating/pH sensing, a polydimethylsiloxane (PDMS) well (size of inner well ~2 × 6 × 6 mm) was attached to the substrates to confine the NaCl or the buffer solutions. (De Oliveira Silva et al., 2019). The saline solution was prepared using NaCl (Sigma Aldrich, 0.1 M) in deionized water. The device fabrication was completed by injecting 0.1 M NaCl aqueous solution in the PDMS well and immersing the activated carbon gate electrode on it (Subramanian et al., 2021). The schematic representation of the device fabrication is shown in **Supplementary Figure S1**. The illustrations of the transistor cross-sections are shown in **Scheme 1**. For pH sensors, the NaCl solution was replaced by different pH buffer solutions (pH of 1.68, 4.01, 7.00, 10.01, and 12.46, Orion pH buffer solutions, Thermo Scientific).

The carbon ink used in the activated carbon gate electrode for the ionic liquid-gated transistors was prepared using activated carbon (Norit CA1, Sigma-Aldrich, 28 mg $ml^{-1}$) and PVDF (Sigma Aldrich, 1.4 mg $ml^{-1}$) in N-methyl pyrrolidone (Sigma Aldrich). The carbon ink used in the activated carbon gate electrode for the aqueous electrolyte-gated transistors was prepared using activated carbon (Norit CA1, Sigma-Aldrich, 28 mg $ml^{-1}$) and Nafion (Sigma Aldrich, 1.4 mg $ml^{-1}$) in isopropyl alcohol. The activated carbon gate electrodes were obtained by drop-casting the carbon ink on the carbon paper (Spectracarb 2050A, Fuel cell store, United States) followed by heating at 60°C for 5 h (Tang et al., 2015; Valitova et al., 2016; De Oliveira Silva et al., 2019).

## Device Characterization

The transistor characterization of IGTs was performed using an electrical probe station equipped with a micropositioner (Signatone Corporation, Gilroy, CA, United States) and a semiconductor parameter analyzer (Keysight B1500A). The electrochemical characterization of $TiO_2$ films was carried out using a potentiostat (VERSASTAT 4, Princeton Applied Research). The electrical and electrochemical characteristics of the ionic liquid gated transistors were measured in a $N_2$ glove box ($H_2O$ <5 ppm and $O_2$ <5 ppm). The electrical and electrochemical characteristics of the aqueous electrolyte-gated transistors were measured in ambient conditions (Subramanian et al., 2021).

## Charge Carrier Density and Mobility Calculations

The charge carrier mobility was extracted from the linear transfer characteristics, using the formula

$$\mu_{lin} = \frac{LI_{ds,lin}}{WenV_{ds}}$$

where $L$ is the interelectrode distance (10 μm), $I_{ds,lin}$ is the drain-source current in the linear regime of transfer characteristics, $W$ is the electrode width (4,000 μm), $e$ is the elementary charge ($1.6 \times 10^{-19}$ C), $V_{ds}$ is the drain-source voltage and $n$ is the charge carrier density. The charge carrier density ($n$) was calculated from the linear transfer characteristics, using the formula

$$n = \frac{Q}{eA} = \frac{\int I_{gs} dV_{gs}}{r_v eA}$$

Where $Q$ is the doping charge, $I_{gs}$ is the gate-source current in the forward scan of the linear transfer characteristics, $r_v$ is the scan rate of the gate-source voltage ($V_{gs}$), and $A$ is the geometric area of the $TiO_2$ films in contact with the ion-gating media (0.36 $cm^2$ for ionic liquid based IGTs and 0.12 $cm^2$ for the aqueous electrolyte-gated IGTs) (Subramanian et al., 2021).

## pH Sensitivity Calculations

The pH sensitivity of IGTs was calculated using gate-source voltage shift with respect to the drain-source current ($10^{-5}$ A) in the forward scan of linear transfer characteristics ($V_{ds}$ = 0.1 V). The gate-source voltage shift ($\Delta V_{gs}$) of IGTs for each pH buffer solution was plotted against the pH value and then the data points were fitted as a straight line by linear regression. The slope (V/pH) of the straight line corresponds to the pH sensitivity (Chou and Liao, 2005; Lee et al., 2020).

# RESULTS AND DISCUSSION

## Film Characterization

Morphological, topographical, and structural properties of $TiO_2$ films were studied before transistor assembly. For films on rigid $SiO_2$/p-Si (route I), SEM images reveal a homogeneous, uniform, and crack-free morphology (**Figure 1A**). The rms roughness was found to be 1.0 ± 0.2 nm (**Figure 1B**). XRD patterns show the presence of the anatase phase (diffraction peak at 2θ ~ 25°, **Figure 1C**). (Subramanian et al., 2020) The additional peaks ~39° and ~45° correspond to metallic gold (originating from the Au patterned electrodes) and aluminum (originating from the substrate holder of the XRD measurement setup). An analogous characterization of $TiO_2$ films on PET (route II) revealed a more granular morphology with a uniform distribution of $TiO_2$ nanoparticles (**Figure 1D**). The rms roughness was found to be 85.4 ± 4.2 nm (**Figure 1E**). Due to the response from the PET substrate at 2θ ~ 25°, the main anatase diffraction peak was not visible in the XRD pattern (**Figure 1F**). The inset of **Figure 1F** shows the magnified pattern with 2θ ranging from 35° to 60°, indicating the presence of both anatase and rutile phases. XRD patterns of route I and route II films are different due to different processing temperatures and different Ti sources (See Experimental).

## Electrochemical Characterization

Cyclic voltammetry was measured in a transistor configuration, with the $TiO_2$ active channel functioning as the working electrode and the activated carbon gate (specific capacitance of ~100 F/g) as the counter and quasi-reference electrode. (Subramanian et al., 2020; Subramanian et al., 2021). The cathodic and anodic signals indicate the doping and dedoping of the $TiO_2$ films. Cyclic voltammograms (CVs) of the route I $TiO_2$ films in [EMIM][TFSI] and 0.1 M NaCl solution, are shown in **Figures 2A,B**. The electrochemical reduction of $TiO_2$ starts around −0.6 V for both [EMIM][TFSI] and 0.1 M aqueous NaCl gating (**Figures 2A,B**). The reduction-oxidation signals are displayed by the wide cathodic and anodic waves. Cyclic voltammograms of route II $TiO_2$ films with [EMIM][TFSI] show that the electrochemical reduction potential of $TiO_2$ starts at ~-1.1 V (See **Supplementary Figure S2** for the cyclic voltammogram in the lower potential window region), which is more cathodic than for route I $TiO_2$ films (~−0.6 V) (**Figure 2C**). This information indicates that the route II $TiO_2$ films can be safely operated between $V_{gs}$ ~ 1 V and $V_{gs}$ ~ 2 V in transistor configuration. As compared to route I $TiO_2$, a higher gate voltage is necessary to activate the channel material, likely due to the lower temperature thermal treatment.

## Ion-Gated Transistors Based on Route I $TiO_2$ Films on $SiO_2$/Si Substrates

The output and transfer characteristics of route I $TiO_2$ films gated with [EMIM][TFSI], measured in a $N_2$–purged glove box, show $n$-type enhancement mode of operation (**Figures 3A,B**). The transfer curve reveals an ON/OFF current ratio of ~$10^3$ (average value of three devices), extracted between $V_{gs}$ = 0 V and $V_{gs}$ = 1.1 V. The hysteresis in the transfer curve is attributed to the slow ion transport during forward and reverse scans. The output and transfer characteristics of route I $TiO_2$ films, gated with 0.1 M NaCl, show a higher drain-source current than the [EMIM][TFSI] counterparts (**Figures 3C,D**). The transfer curves shows that the ON/OFF current ratio of the transistors, calculated between $V_{gs}$ = 0 V and $V_{gs}$ = 1.1 V, is ~$10^4$ (average value of three devices). Compared to the [EMIM][TFSI]-gated devices, $NaCl_{(aq)}$-gated transistors show a clearer drain current saturation as well as a lower hysteresis, likely due to the faster dedoping. The charge carrier density and charge carrier mobility were ~$1.7 \times 10^{14}$ $cm^{-2}$ and ~$3.5 \times 10^{-2}$ $cm^2$/Vs for [EMIM][TFSI] gated devices and ~$1.5 \times 10^{16}$ $cm^{-2}$ and ~$4.5 \times 10^{-3}$ $cm^2$/Vs for the NaCl gated ones. The obtained mobility values (average values of three devices) are comparable with the previous articles based on metal oxide TFTs and IGTs (Wöbkenberg et al., 2010; Liang et al., 2012; Zhong et al., 2012; De Oliveira Silva et al., 2019).

## pH Sensors Based on Ion-Gated $TiO_2$ Films

Low voltage operation in aqueous media makes $TiO_2$ IGTs suitable for ion-sensing applications. With the aim to demonstrate pH sensing, we used $TiO_2$ IGTs with pH buffer solutions as the ion-gating media.

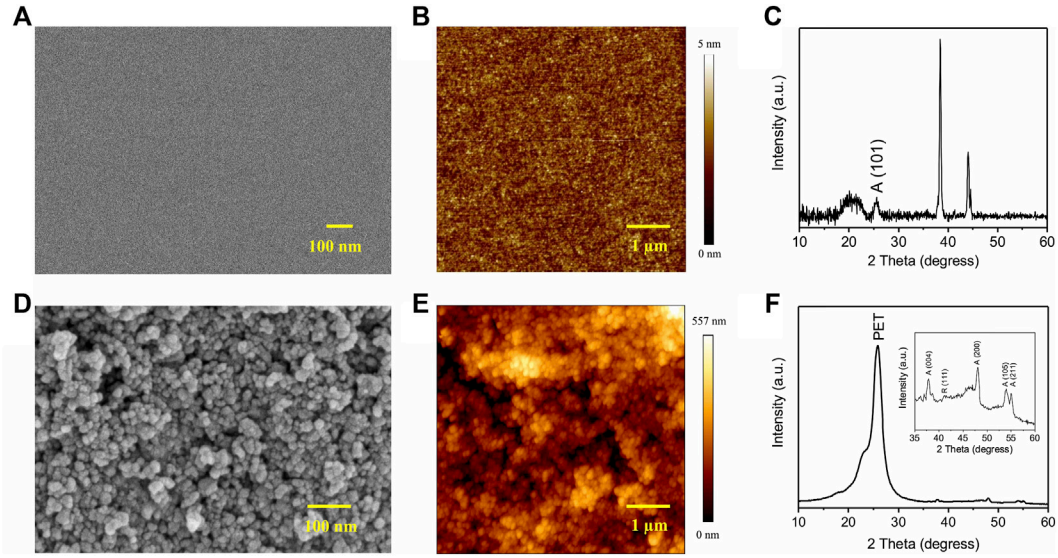


**FIGURE 1 | (A,D)** SEM images, **(B, E)** AFM images and **(C, F)** XRD patterns of $TiO_2$ films on $SiO_2$/*p*-Si **(A–C)** and PET **(D–F)** substrates prepared by route I and route II. A and R indicate anatase and rutile phases of $TiO_2$.

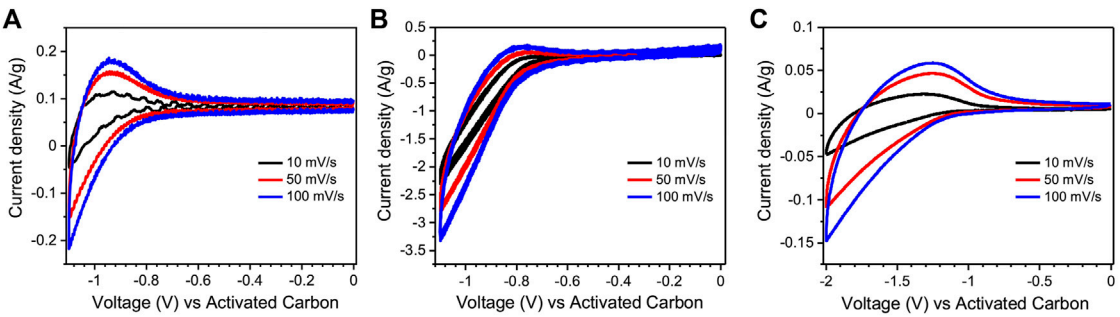


**FIGURE 2 |** Cyclic voltammetry in transistor configuration for route I $TiO_2$ films gated with [EMIM][TFSI] **(A)** and 0.1 M NaCl **(B)**, and route II $TiO_2$ films gated with [EMIM][TFSI] **(C)**. The scan rates are 10, 50, and 100 mV/s.

**Figure 4A** shows the forward transfer characteristics ($V_{ds}$ = 0.1 V) of the IGT gated with pH buffer solutions (pH from 1.68 to 12.48). Two additional set of data extracted from two other devices are shown in **Supplementary Figure S3**. The change of pH of the gating media leads to a shift of the gate voltage at a given reference drain-source current point (e.g., $I_{ds} = 10^{-5}$ A). Being $TiO_2$ an n-type semiconductor, when a positive voltage is applied to the gate electrode of $TiO_2$ IGTs, the positive ions in the gating medium migrate and accumulates on the surface of $TiO_2$ films, leading to an increase in electron density. Therefore, the negative shift in gate voltage observed when lowering the pH of ion-gating media, can be attributed to the increase of the of $H_3O^+$ concentration. The gate voltage shift at $10^{-5}$ A plotted against pH (**Figure 4B**) shows a pH sensitivity of $TiO_2$ IGTs of ~48 mV/pH (average value of 3 devices), which is comparable with the pH sensitivity values of metal oxide IGT based pH sensors (Bhatt et al., 2020; Lee et al., 2020; Woo Son et al., 2020). A larger statistical difference in gate voltage shift is observed for $TiO_2$ IGTs at higher pH levels. The forward and backward scan of transfer characteristics of the $TiO_2$ IGTs with an increasing pH value does not show any significant hysteresis (**Supplementary Figure S4**). The transfer characteristics of $TiO_2$ IGTs measured with a decreasing pH value shows the same trend in device response with respect to increasing pH (**Supplementary Figure S5**).

## Ion-Gated Transistors Based on Route II $TiO_2$ Films on PET Substrates

Transistors processed by route II synthesis on flexible PET substrates, characterized under flat and bent state using [EMIM][TFSI] as the gating medium. **Figure 5** shows the output (A–C) and transfer (D, E) characteristics. These transistors required a higher voltage compared to the route I

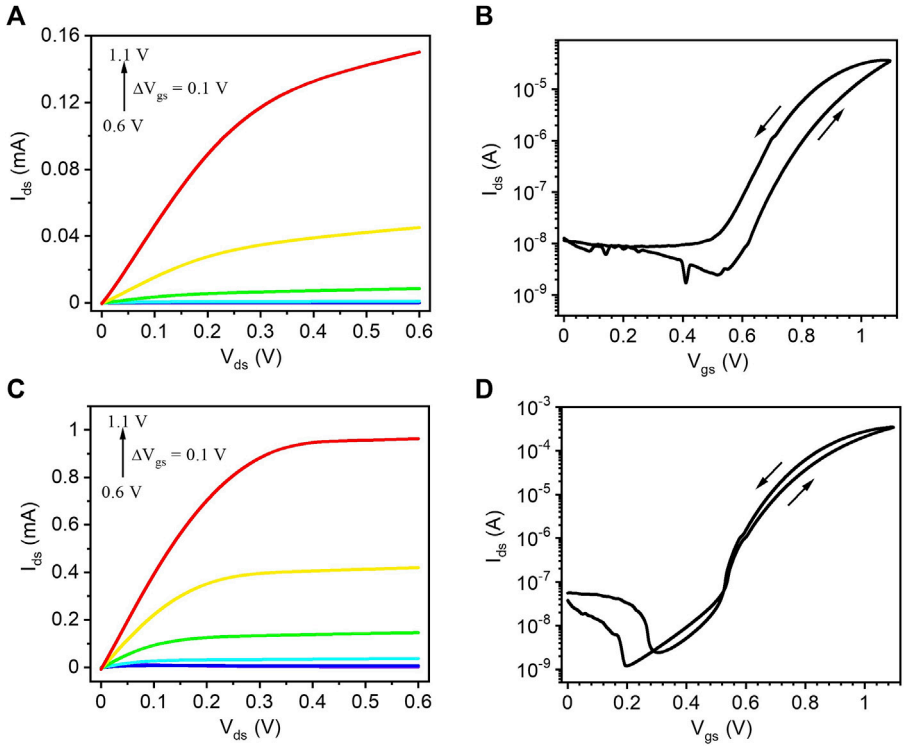


**FIGURE 3 | (A,C)** Output and **(B,D)** transfer characteristics of route I $TiO_2$ films on $SiO_2$/p-Si substrates gated with [EMIM][TFSI], measured in a $N_2$-purged glove box **(A,B)** and with 0.1M $NaCl_{(aq)}$ measured in ambient conditions **(C,D)**. The output characteristics were measured at $V_{gs}$ = 0.6, 0.7, 0.8, 0.9, 1.0, and 1.1 V and the transfer characteristics at $V_{ds}$ = 0.1 V with a scan rate of 10 mV/s.

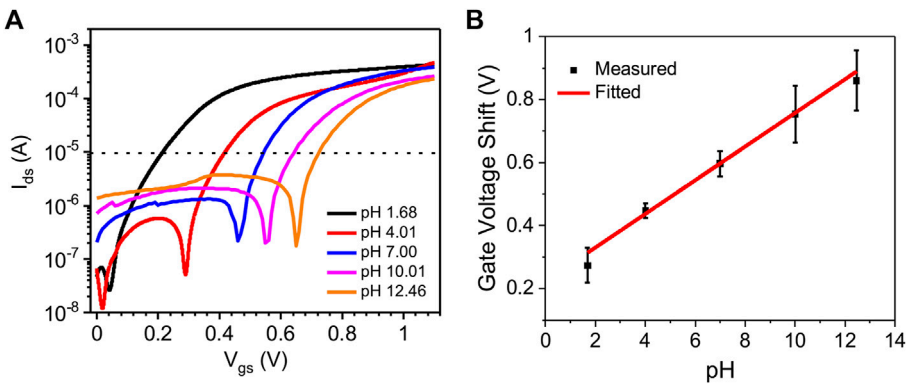


**FIGURE 4 | (A)** Transfer (forward scan) characteristics ($V_{ds}$ = 0.1 V) of route I $TiO_2$ films on $SiO_2$/Si substrates gated with pH buffer (pH 1.68, 4.01, 7.00, 10.01, and 12.46) solutions measured in ambient air. The $V_{gs}$ scan rate is 10 mV/s. **(B)** Gate voltage shift corresponding to the reference drain-source current point (ca $10^{-5}$ A) versus pH. Each point in Figure 4 **(B)** corresponds to the average gate voltage shift of 3 devices with respect to pH value. The error bar in the graph indicates the standard deviation of 3 devices.

ones, in agreement with cyclic voltammetry data discussed above (**Figure 2C**). For comparison, we prepared similar devices on $SiO_2$/Si substrates, which did not show any significant difference in the transistor characteristics with respect to PET substrates (**Supplementary Figure S6**). Compared to the route I devices, we observed a higher turn on voltage for route II devices, likely due to the lower processing temperature of $TiO_2$. The linear transfer characteristics from $V_{gs}$ = −2 V to $V_{gs}$ = +2 V do not show any p-type transistor behavior (**Supplementary Figure S7**). Route II $TiO_2$ shows a lower saturation current as compared to the route I $TiO_2$. The charge carrier density and charge carrier mobility, extracted from the linear transfer characteristics (**Figure 5D**), were ~$1.2 \times 10^{15}$ $cm^{-2}$ and $7.5 \times 10^{-3}$ $cm^2$/Vs (average value of three devices). The ON/OFF ratio, extracted from the saturation

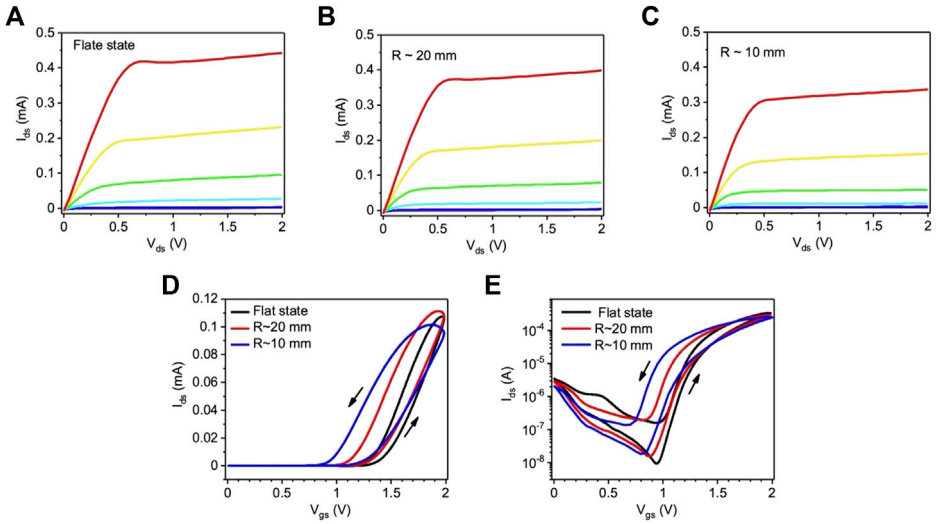


**FIGURE 5 | (A–C)** Output and **(D,E)** transfer characteristics of route II $TiO_2$ films on PET substrates gated with [EMIM] [TFSI] measured in a $N_2$ purged glove box. The output characteristics under **(A)** flat, **(B)** bending radius ~20 mm and **(C)** bending radius ~10 mm were measured at $V_{gs}$ = 0, 1.0, 1.25, 1.5, 1.75, and 2.0 V. The transfer characteristics under flat and bent state were measured in **(D)** linear ($V_{ds}$ = 0.2 V) and **(E)** saturation ($V_{ds}$ = 1.75 V) regime. The scan rate is 50 mV/s.

transfer characteristics (**Figure 5E**), extracted between $V_{gs}$ = 0 V and $V_{gs}$ = 2 V, was ~ $10^2$ (average value of three devices). Transistor characterization under tensile bending radii at R ~ 20 mm (**Figure 5B**) and at R ~ 10 mm (**Figure 5C**) shows a slight decrease in $I_{ds}$ and their ON/OFF ratio (**Figure 5E**) is not severely affected by the bending. The device characteristics under flat state after bending are shown in **Supplementary Figure S8**. The drain-source current is slightly recovered after the bending measurements. The saturation transfer characteristics after multiple bending cycles shows no significant change with respect to the unbent state (**Supplementary Figure S9**). Two additional set of data (saturation transfer characteristics) extracted from two other devices are shown in **Supplementary Figure S10**.

The operating voltage of route II devices lays beyond the thermodynamical stability window of water, therefore preventing their use in the aqueous gating medium, as the high voltage may causes unwanted redox processes.

## CONCLUSION AND PERSPECTIVES

We fabricated $TiO_2$ films on rigid and flexible substrates using sustainable wet synthesis. We demonstrated the transistor behavior of $TiO_2$ films using room temperature ionic liquid and aqueous saline solution. $TiO_2$ IGTs were successfully used as pH sensors with a sensitivity of ~48 mV/pH. Furthermore, $TiO_2$ films were deposited on the flexible PET substrates at the maximum processing temperature of 120°C. The transistor behavior of $TiO_2$ IGTs was not severely affected by the tensile bending radii (R ~ 20 mm and R ~ 10 mm). In view of the flexibility and low temperature processability, route II $TiO_2$ IGTs pave the way to future low-cost flexible electronics. Currently, work is in progress to fabricate $TiO_2$ thin films on flexible substrates using controlled aqueous growth at lower temperatures for flexible pH sensing applications.

## DATA AVAILABILITY STATEMENT

The raw data supporting the conclusion of this article will be made available by the authors, without undue reservation.

## AUTHOR CONTRIBUTIONS

FC and AS designed the experiments. AS performed the transistor and electrochemical characteristics of the devices. FC supervised the experiments. CL did SEM, AFM and XRD characterizations. MA did AFM characterization and pH sensing measurements. SL and CS revised the manuscript.

## ACKNOWLEDGMENTS

The Natural Sciences and Engineering Research Council of Canada (NSERC) is acknowledged for a Discovery Grant (F.C.). Equipment and infrastructure used for this research were acquired and maintained by the Canada Foundation for Innovation and Quebec Strategic Networks (CQMF-QCAM, RQMP, CREPEC, and GCM), respectively. AS and MA are grateful to the Trottier Energy Institute for a doctoral scholarship. AS is grateful to the FRQNT for a doctoral scholarship. CL is grateful to the Polytechnique Montréal for a research internship scholarship.

## SUPPLEMENTARY MATERIAL

The Supplementary Material for this article can be found online at: https://www.frontiersin.org/articles/10.3389/felec.2022.813535/full#supplementary-material

## REFERENCES


AlQahtani, H., Alswieleh, A., Al-Khurayyif, I., AlGarni, S., and Grell, M. (2021). Parallel Potentiometric and Capacitive Response in a Water-Gate Thin Film Transistor Biosensor at High Ionic Strength. *Sensors* 21 (16), 5618. doi:10.3390/s21165618

Anitha, V. C., Banerjee, A. N., and Joo, S. W. (2015). Recent Developments in TiO2 as N- and P-type Transparent Semiconductors: Synthesis, Modification, Properties, and Energy-Related Applications. *J. Mater. Sci.* 50 (23), 7495–7536. doi:10.1007/s10853-015-9303-7

Asare, J., Agyei-Tuffour, B., Amonoo, E. A., Dodoo-Arhin, D., Nyankson, E., Mensah, B., et al. (2020). Effects of Substrates on the Performance of Optoelectronic Devices: A Review. *Cogent Eng.* 7 (1), 1829274. doi:10.1080/23311916.2020.1829274

Azimi, M., Subramanian, A., Roslan, N. A., and Cicoira, F. (2021). Flexible Organic Ion-Gated Transistors with Low Operating Voltage and Light-Sensing Application. *J. Phys. Mater.* 4 (2), 024001. doi:10.1088/2515-7639/abd018

Baeg, K. J., and Lee, J. (2020). Flexible Electronic Systems on Plastic Substrates and Textiles for Smart Wearable Technologies. *Adv. Mater. Technol.* 5 (7), 2000071. doi:10.1002/admt.202000071

Bandiello, E., Sessolo, M., and Bolink, H. J. (2014). Aqueous Electrolyte-Gated ZnO Transistors for Environmental and Biological Sensing. *J. Mater. Chem. C* 2 (48), 10277–10281. doi:10.1039/c4tc02075h

Bhatt, D., Kumar, S., and Panda, S. (2020). Amorphous IGZO Field Effect Transistor Based Flexible Chemical and Biosensors for Label Free Detection. *Flex. Print. Electron.* 5 (1), 014010. doi:10.1088/2058-8585/ab724c

Bisri, S. Z., Shimizu, S., Nakano, M., and Iwasa, Y. (2017). Endeavor of Iontronics: From Fundamentals to Applications of Ion-Controlled Electronics. *Adv. Mater.* 29 (25), 1607054. doi:10.1002/adma.201607054

Bu, X., Xu, H., Shang, D., Li, Y., Lv, H., and Liu, Q. (2020). Ion-Gated Transistor: An Enabler for Sensing and Computing Integration. *Adv. Intell. Syst.* 2, 2000156. doi:10.1002/aisy.202000156

Cadilha Marques, G., Weller, D., Erozan, A. T., Feng, X., Tahoori, M., and Aghassi-Hagmann, J. (2019). Progress Report on "From Printed Electrolyte-Gated Metal-Oxide Devices to Circuits". *Adv. Mater.* 31 (26), 1806483. doi:10.1002/adma.201806483

Cea, C., Spyropoulos, G. D., Jastrzebska-Perfect, P., Ferrero, J. J., Gelinas, J. N., and Khodagholy, D. (2020). Enhancement-mode Ion-Based Transistor as a Comprehensive Interface and Real-Time Processing Unit for *In Vivo* Electrophysiology. *Nat. Mater.* 19 (6), 679–686. doi:10.1038/s41563-020-0638-3

Chang, H.-K., Ishikawa, F. N., Zhang, R., Datar, R., Cote, R. J., Thompson, M. E., et al. (2011). Rapid, Label-free, Electrical Whole Blood Bioassay Based on Nanobiosensor Systems. *ACS Nano* 5 (12), 9883–9891. doi:10.1021/nn2035796

Chen, X., and Selloni, A. (2014). Introduction: Titanium Dioxide ($TiO_2$) Nanomaterials. *Chem. Rev.* 114 (19), 9281–9282. doi:10.1021/cr500422r

Chong, H. Y., and Kim, T. W. (2013). Electrical Characteristics of Thin-Film Transistors Fabricated Utilizing a UV/Ozone-Treated TiO2 Channel Layer. *J. Elec Materi* 42 (3), 398–402. doi:10.1007/s11664-012-2348-3

Chou, J.-C., and Liao, L. P. (2005). Study on pH at the point of Zero Charge of TiO2 pH Ion-Sensitive Field Effect Transistor Made by the Sputtering Method. *Thin Solid Films* 476 (1), 157–161. doi:10.1016/j.tsf.2004.09.061

De A. Freire, M. T., Castle, L., Reyes, F. G. R., and Reyes, F. G. (1999). Thermal Stability of Polyethylene Terephthalate (PET): Oligomer Distribution and Formation of Volatiles. *Packag. Technol. Sci.* 12 (1), 29–36. doi:10.1002/(sici)1099-1522(199901/02)12:1<29::aid-pts451>3.0.co;2-d

De Oliveira Silva, G. V., Subramanian, A., Meng, X., Zhang, S., Barbosa, M. S., Baloukas, B., et al. (2019). Tungsten Oxide Ion-Gated Phototransistors Using Ionic Liquid and Aqueous Gating media. *J. Phys. D: Appl. Phys.* 52 (30), 305102. doi:10.1088/1361-6463/ab1dbb

Griffin, J. M. (2020). A Gateway to Understanding Confined Ions. *Nat. Nanotechnol.* 15 (8), 628–629. doi:10.1038/s41565-020-0709-2

Horita, R., Ohtani, K., Kai, T., Murao, Y., Nishida, H., Toya, T., et al. (2013). Transport Properties of Anatase-TiO2Polycrystalline-Thin-Film Field-Effect Transistors with Electrolyte Gate Layers. *Jpn. J. Appl. Phys.* 52 (11R), 115803. doi:10.7567/jjap.52.115803

Huang, W., Chen, J., Wang, G., Yao, Y., Zhuang, X., Pankow, R. M., et al. (2021). Dielectric Materials for Electrolyte Gated Transistor Applications. *J. Mater. Chem. C* 9 (30), 9348–9376. doi:10.1039/d1tc02271g

Ishikawa, F. N., Chang, H.-K., Curreli, M., Liao, H.-I., Olson, C. A., Chen, P.-C., et al. (2009). Label-free, Electrical Detection of the SARS Virus N-Protein with Nanowire Biosensors Utilizing Antibody Mimics as Capture Probes. *ACS Nano* 3 (5), 1219–1224. doi:10.1021/nn900086c

Ji, D., Jang, J., Park, J. H., Kim, D., Rim, Y. S., Hwang, D. K., et al. (2021). Recent Progress in the Development of Backplane Thin Film Transistors for Information Displays. *J. Inf. Display* 22 (1), 1–11. doi:10.1080/15980316.2020.1818641

Kajitvichyanukul, P., Ananpattarachai, J., and Pongpom, S. (2005). Sol–gel Preparation and Properties Study of TiO2 Thin Film for Photocatalytic Reduction of Chromium (VI) in Photocatalysis Process. *Sci. Tech. Adv. Mater.* 6 (3-4), 352. doi:10.1016/j.stam.2005.02.014

Kergoat, L., Herlogsson, L., Braga, D., Piro, B., Pham, M.-C., Crispin, X., et al. (2010). A Water-Gate Organic Field-Effect Transistor. *Adv. Mater.* 22 (23), 2565–2569. doi:10.1002/adma.200904163

Kim, H., and Hwang, T. (2014). Effect of Titanium Isopropoxide Addition in Low-Temperature Cured TiO2 Photoanode for a Flexible DSSC. *J. Sol-gel Sci. Technol.* 72 (1), 67–73. doi:10.1007/s10971-014-3427-0

Kim, S. H., Hong, K., Xie, W., Lee, K. H., Zhang, S., Lodge, T. P., et al. (2013). Electrolyte-Gated Transistors for Organic and Printed Electronics. *Adv. Mater.* 25 (13), 1822–1846. doi:10.1002/adma.201202790

Laiho, A., Herlogsson, L., Forchheimer, R., Crispin, X., and Berggren, M. (2011). Controlling the Dimensionality of Charge Transport in Organic Thin-Film Transistors. *Proc. Natl. Acad. Sci.* 108 (37), 15069–15073. doi:10.1073/pnas.1107063108

Lee, S., Park, S., Kim, C.-H., and Yoon, M.-H. (2020). Approaching the Nernst Detection Limit in an Electrolyte-Gated Metal Oxide Transistor. *IEEE Electron. Device Lett.* 42 (1), 50–53. doi:10.1109/led.2020.3040149

Leighton, C. (2019). Electrolyte-based Ionic Control of Functional Oxides. *Nat. Mater* 18 (1), 13–18. doi:10.1038/s41563-018-0246-7

Li, J.-Y., Chang, S.-P., Chang, S.-J., and Tsai, T.-Y. (2014). Sensitivity of EGFET pH Sensors with TiO2 Nanowires. *ECS Solid State. Lett.* 3 (10), P123–P126. doi:10.1149/2.0091410ssl

Liang, F., Luo, L.-B., Tsang, C.-K., Zheng, L., Cheng, H., and Li, Y. Y. (2012). TiO2 Nanotube-Based Field Effect Transistors and Their Application as Humidity Sensors. *Mater. Res. Bull.* 47 (1), 54–58. doi:10.1016/j.materresbull.2011.10.006

Manjakkal, L., Szwagierczak, D., and Dahiya, R. (2020). Metal Oxides Based Electrochemical pH Sensors: Current Progress and Future Perspectives. *Prog. Mater. Sci.* 109, 100635. doi:10.1016/j.pmatsci.2019.100635

Moonen, P. F., Yakimets, I., and Huskens, J. (2012). Fabrication of Transistors on Flexible Substrates: from Mass-Printing to High-Resolution Alternative Lithography Strategies. *Adv. Mater.* 24 (41), 5526–5541. doi:10.1002/adma.201202949

Nomura, K., Ohta, H., Takagi, A., Kamiya, T., Hirano, M., and Hosono, H. (2004). Room-temperature Fabrication of Transparent Flexible Thin-Film Transistors Using Amorphous Oxide Semiconductors. *Nature* 432 (7016), 488–492. doi:10.1038/nature03090

Nunes, D., Pimentel, A., Gonçalves, A., Pereira, S., Branquinho, R., Barquinha, P., et al. (2019). Metal Oxide Nanostructures for Sensor Applications. *Semicond. Sci. Technol.* 34 (4), 043001. doi:10.1088/1361-6641/ab011e

Papac, M., Stevanović, V., Zakutayev, A., and O'Hayre, R. (2021). Triple Ionic-Electronic Conducting Oxides for Next-Generation Electrochemical Devices. *Nat. Mater.* 20 (3), 301–313. doi:10.1038/s41563-020-00854-8

Park, J. W., Kang, B. H., and Kim, H. J. (2020). A Review of Low-Temperature Solution-Processed Metal Oxide Thin-Film Transistors for Flexible Electronics. *Adv. Funct. Mater.* 30 (20), 1904632. doi:10.1002/adfm.201904632

Parthiban, S., Anuratha, K. S., Arunprabaharan, S., Abinesh, S., and Lakshminarasimhan, N. (2015). Enhanced Dye-Sensitized Solar Cell Performance Using TiO2:Nb Blocking Layer Deposited by Soft Chemical Method. *Ceramics Int.* 41 (1), 205–209. doi:10.1016/j.ceramint.2014.08.059

Ramarajan, R., Paul Joseph, D., Thangaraju, K., and Kovendhan, M. (2020). Indium-Free Alternative Transparent Conducting Electrodes: An Overview and Recent Developments. *Metal Metal Oxides Energ. Elect.* 55, 149–183. doi:10.1007/978-3-030-53065-5_5

Rim, Y. S. (2020). Review of Metal Oxide Semiconductors-Based Thin-Film Transistors for point-of-care Sensor Applications. *J. Inf. Display* 21, 1–8. doi:10.1080/15980316.2020.1714762

Sedki, M., Shen, Y., and Mulchandani, A. (2021). Nano-FET-enabled Biosensors: Materials Perspective and Recent Advances in North America. *Biosens. Bioelectron.* 176, 112941. doi:10.1016/j.bios.2020.112941

Şerban, I., and Enesca, A. (2020). Metal Oxides-Based Semiconductors for Biosensors Applications. *Front. Chem.* 8, 354. doi:10.3389/fchem.2020.00354

Shi, J., Zhang, J., Yang, L., Qu, M., Qi, D.-C., and Zhang, K. H. (2021). Wide Bandgap Oxide Semiconductors: from Materials Physics to Optoelectronic Devices. *Adv. Mater.* 33, e2006230. doi:10.1002/adma.202006230

Singh, M., Mulla, M. Y., Santacroce, M. V., Magliulo, M., Di Franco, C., Manoli, K., et al. (2016). Effect of the Gate Metal Work Function on Water-Gated ZnO Thin-Film Transistor Performance. *J. Phys. D: Appl. Phys.* 49 (27), 275101. doi:10.1088/0022-3727/49/27/275101

Song, J., Huang, X., Han, C., Yu, Y., Su, Y., and Lai, P. (2021). Recent Developments of Flexible InGaZnO Thin-Film Transistors. *Phys. Status Solidi A.* 218 (7), 2000527. doi:10.1002/pssa.202000527

Sood, A., Poletayev, A. D., Cogswell, D. A., Csernica, P. M., Mefford, J. T., Fraggedakis, D., et al. (2021). Electrochemical Ion Insertion from the Atomic to the Device Scale. *Nat. Rev. Mater.* 6, 1–21. doi:10.1038/s41578-021-00314-y

Subramanian, A., George, B., Bobbara, S. R., Valitova, I., Ruggeri, I., Borghi, F., et al. (2020). Ion-gated Transistors Based on Porous and Compact TiO2 Films: Effect of Li Ions in the Gating Medium. *AIP Adv.* 10 (6), 065314. doi:10.1063/5.0009984

Subramanian, A., Azimi, M., Santato, C., and Cicoira, F. (2021). Combining Aqueous Solution Processing and Printing for Fabrication of Flexible and Sustainable Tin Dioxide Ion-Gated Transistors. *Adv. Mater. Tech.* 7, 2100843. doi:10.1002/admt.202100843

Tang, H., Kumar, P., Zhang, S., Yi, Z., Crescenzo, G. D., Santato, C., et al. (2015). Conducting Polymer Transistors Making Use of Activated Carbon Gate Electrodes. *ACS Appl. Mater. Inter.* 7 (1), 969–973. doi:10.1021/am507708c

Thomas, S. R., Pattanasattayavong, P., and Anthopoulos, T. D. (2013). Solution-processable Metal Oxide Semiconductors for Thin-Film Transistor Applications. *Chem. Soc. Rev.* 42 (16), 6910–6923. doi:10.1039/c3cs35402d

Tiwale, N., Subramanian, A., Dai, Z., Sikder, S., Sadowski, J. T., and Nam, C.-Y. (2020). Large Mobility Modulation in Ultrathin Amorphous Titanium Oxide Transistors. *Commun. Mater.* 1 (1), 1–8. doi:10.1038/s43246-020-00096-w

Tiwari, N., Nirmal, A., Kulkarni, M. R., John, R. A., and Mathews, N. (2020). Enabling High Performance N-type Metal Oxide Semiconductors at Low Temperatures for Thin Film Transistors. *Inorg. Chem. Front.* 7 (9), 1822–1844. doi:10.1039/d0qi00038h

Torricelli, F., Adrahtas, D. Z., Bao, Z., Berggren, M., Biscarini, F., Bonfiglio, A., et al. (2021). Electrolyte-gated Transistors for Enhanced Performance Bioelectronics. *Nat. Rev. Methods Primers* 1 (1), 1–24. doi:10.1038/s43586-021-00065-8

Valitova, I., Kumar, P., Meng, X., Soavi, F., Santato, C., and Cicoira, F. (2016). Photolithographically Patterned TiO2 Films for Electrolyte-Gated Transistors. *ACS Appl. Mater. Inter.* 8 (23), 14855–14862. doi:10.1021/acsami.6b01922

Wager, J. F. (2016). Oxide TFTs: A Progress Report. *Inf. Display* 32 (1), 16–21. doi:10.1002/j.2637-496x.2016.tb00871.x

Wager, J. F. (2020). TFT Technology: Advancements and Opportunities for Improvement. *Inf. Display* 36 (2), 9–13. doi:10.1002/msid.1098

Wang, Y., Sun, L., Wang, C., Yang, F., Ren, X., Zhang, X., et al. (2019). Organic Crystalline Materials in Flexible Electronics. *Chem. Soc. Rev.* 48 (6), 1492–1530. doi:10.1039/c8cs00406d

Wöbkenberg, P. H., Ishwara, T., Nelson, J., Bradley, D. D., Haque, S. A., and Anthopoulos, T. D. (2010). TiO 2 Thin-Film Transistors Fabricated by spray Pyrolysis. *Appl. Phys. Lett.* 96 (8), 082116. doi:10.1063/1.3330944

Woo Son, H., Park, J. H., Chae, M.-S., Kim, B.-H., and Kim, T. G. (2020). Bilayer Indium Gallium Zinc Oxide Electrolyte-Gated Field-Effect Transistor for Biosensor Platform with High Reliability. *Sensors Actuators B: Chem.* 312, 127955. doi:10.1016/j.snb.2020.127955

Yajima, T., Oike, G., Nishimura, T., and Toriumi, A. (2016). Independent Control of Phases and Defects in TiO2thin Films for Functional Transistor Channels. *Phys. Status Solidi A.* 213 (8), 2196–2202. doi:10.1002/pssa.201600006

Yao, P.-C., Chiang, J.-L., and Lee, M.-C. (2014). Application of Sol-Gel TiO2 Film for an Extended-Gate H+ Ion-Sensitive Field-Effect Transistor. *Solid State. Sci.* 28, 47–54. doi:10.1016/j.solidstatesciences.2013.12.011

Yoo, H., Lee, I. S., Jung, S., Rho, S. M., Kang, B. H., and Kim, H. J. (2021). A Review of Phototransistors Using Metal Oxide Semiconductors: Research Progress and Future Directions. *Adv. Mater.* 33, 2006091. doi:10.1002/adma.202006091

Yusof, K. A., Abdul Rahman, R., Zulkefle, M. A., Herman, S. H., and Abdullah, W. F. H. (2016). EGFET pH Sensor Performance Dependence on Sputtered TiO2 Sensing Membrane Deposition Temperature. *J. Sensors* 2016, 1–9. doi:10.1155/2016/7594531

Zardetto, V., Brown, T. M., Reale, A., and Di Carlo, A. (2011). Substrates for Flexible Electronics: A Practical Investigation on the Electrical, Film Flexibility, Optical, Temperature, and Solvent Resistance Properties. *J. Polym. Sci. B Polym. Phys.* 49 (9), 638–648. doi:10.1002/polb.22227

Zhang, J., Zhang, Y., Cui, P., Lin, G., Ni, C., and Zeng, Y. (2021). One-Volt $TiO_2$ Thin Film Transistors with Low-Temperature Process. *IEEE Electron. Device Lett.* 42 (4), 521–524. doi:10.1109/led.2021.3060973

Zhong, N., Cao, J. J., Shima, H., and Akinaga, H. (2012). Effect of Annealing Temperature on $\hbox{TiO}_{2}$ -Based Thin-Film-Transistor Performance. *IEEE Electron. Device Lett.* 33 (7), 1009–1011. doi:10.1109/led.2012.2193658

Zulkefle, M. A., Abdul Rahman, R., Yusof, K. A., Abdullah, W. F. H., Rusop, M., and Herman, S. H. (2016). Spin Speed and Duration Dependence of TiO2 Thin Films pH Sensing Behavior. *J. Sensors* 2016, 1–8. doi:10.1155/2016/9746156

**Conflict of Interest:** The authors declare that the research was conducted in the absence of any commercial or financial relationships that could be construed as a potential conflict of interest.

**Publisher's Note:** All claims expressed in this article are solely those of the authors and do not necessarily represent those of their affiliated organizations, or those of the publisher, the editors and the reviewers. Any product that may be evaluated in this article, or claim that may be made by its manufacturer, is not guaranteed or endorsed by the publisher.